Accepted Manuscript

Micro Additive Manufacturing of Glucose Biosensors: A Feasibility Study

Sepehr Nesaei, Yang Song, Yijia Wang, Xiaofan Ruan, Dan Du, Arda Gozen, Yuehe Lin

PII: S0003-2670(18)31070-5

DOI: 10.1016/j.aca.2018.09.012

Reference: ACA 236248

To appear in: *Analytica Chimica Acta*

Received Date: 14 June 2018

Revised Date: 2 September 2018

Accepted Date: 5 September 2018

Please cite this article as: S. Nesaei, Y. Song, Y. Wang, X. Ruan, D. Du, A. Gozen, Y. Lin, Micro Additive Manufacturing of Glucose Biosensors: A Feasibility Study, *Analytica Chimica Acta* (2018), doi: 10.1016/j.aca.2018.09.012.

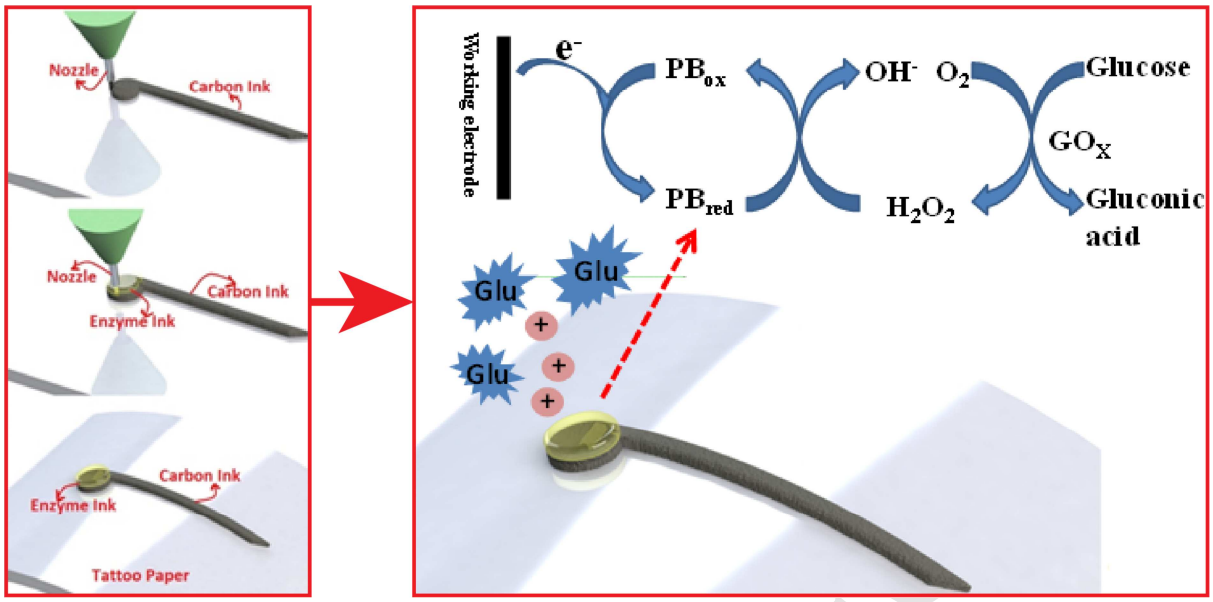

Micro Additive Manufacturing of Glucose Biosensors: A Feasibility Study

Sepehr Nesaei[1], Yang Song [1], Yijia Wang, Xiaofan Ruan, Dan Du, Arda Gozen* and Yuehe Lin*

School of Mechanical and Materials Engineering, Washington State University, Pullman, WA 99164

Keywords: Additive Manufacturing, electrochemical biosensors, Direct-Ink-Writing, glucose

ABSTRACT

Flexible electrochemical sensors for measurement and quantification of biomarkers are attracting a great deal of attention in non-invasive medical applications, due to their high mechanical compatibility and conformability with the human body. Realization of the full potential of such novel systems relies heavily on their effective manufacturing. Particularly, there is a need for manufacturing techniques that can realize complex designs, consisting of multiple functional materials which are required for sensor functionality. Among emerging additive manufacturing techniques, Direct-Ink-Writing (DIW), where polymer nanocomposite inks are dispensed through nozzles and deposited with high spatial control, carries a great potential to address this need. Here, we introduce a 3D printed flexible electrochemical biosensor for glucose detection. We show that our biosensor works linearly in glucose solution with a concentration range between 100 and 1000 µM. The sensitivity of glucose biosensor is estimated to be 17.5 nA μM^{-1} and the calculated value of detection limit (S/N= 3) is 6.9 µM. The demonstrated electrochemical performance and surface properties of the printed sensors show the promising advantages of using this technique over conventional screen printing method. These advantages include higher sensitivity and specificity and, reduced material consumption.

1. INTRODUCTION

Over the past decades, glucose biosensors have attracted intense research interest because of their value in diabetes management [1]. The personalized nature of this problem renders the several conventional glucose detection methods such as fluorescence and colorimetric strategies as unsuitable for the trace analysis of glucose in human body[2–4]. The most commonly used personalized blood glucose level measurement method involves using a commercial glucose meter requiring frequent pricking of fingertips. Alternative methods involve using of continuous glucose monitoring systems, however these systems are expensive and need frequently changing invasive needle/sensor insertions [5]. Nowadays, extensive efforts have been aimed at developing wearable electronics and their applications in biomedical fields. Specific emphasis has been placed on developing non-invasive monitoring of other body fluids such as human sweat [6–9]. One of the examples shown recently is the use of wearable patches to simultaneously track the levels of metabolites and electrolytes in human sweat [10].

In developing wearable sensors, several factors should be considered, including mechanical flexibility for conformance to the human body, device scalability and miniaturized electronics and devices [11,12]. Traditional manufacturing strategies are typically based on adaptations of conventional 2D fabrication processes, such as spin coating, photolithography and screen-printing [13,14]. These approaches have been shown to be appropriate for recently emerging wearable biosensors [15–17]. Despite their demonstrated feasibility, there are many drawbacks in using such techniques including the use of harmful chemicals, rigorous fabrication steps, material waste, the need for expensive cleanroom processing and failure to integrate enzyme/electrode co-production. Thus, further research effort is still needed for the development of new processes with higher levels of customizability, higher throughput and reduced material waste.

Emerging additive manufacturing techniques can address these issues as they offer many opportunities for various critical technologies including wearable electronics [18], energy storage [19], artificial tissue engineering [20] and food fabrication [21]. Among these methods, Direct-Ink-Writing (DIW) involves dispensing “inks” out of nozzles within the range of mm to µm scale and depositing them with high levels of spatial control and accuracy. These inks typically contain functional materials with tunable rheological properties. Complex designs are achieved through pre-defined digitalized paths [22]. DIW is able to process a myriad of ink materials such as suspensions [23], polymer melts [24] and solutions [25], hydrogels including living cells [20] and metals [26]. More recently, the DIW’s capability of directing nanoparticle morphology during printing of composite inks. This capability enables DIW to control the properties of the printed structures [27,28]. One of the most prominent applications of the DIW technology is printing of electrically conductive nano-composites to fabricate mechanically compliant electrodes [29,30]. This unique capability has been utilized in various applications including electrochemical energy storage [31]. The versatility of the DIW approach also enables fabrication of multi-material functionally-graded structures in wide range

of size scales. Combination of this capability with the demonstrated success of DIW in processing conductive nanocomposites into flexible electrodes carries a great potential in manufacturing of wearable biosensors, which require precise integration of multiple active materials in well controlled electrode geometries. This paper explores this potential which has not yet been realized. Specifically, the presented study is the first example of using DIW for electrochemical sensing through the printing of multiple materials for synergistic functionally.

Here, a feasibility study of micro additive manufacturing of glucose biosensor is presented. A novel dual 3D printing of Prussian blue modified electrode and glucose oxidase enzyme layer for electrochemical biosensing has been introduced (**Scheme 1**). The performance of the printed electrodes has been compared to screen-printed counterparts having the same material composition and geometry. Electrodes were 3D printed in different sizes and electrochemical measurements were performed to study the effect of the electrode diameter, which is precisely and flexibly controlled through 3D printing, on the sensor performance.

2. EXPERIMENTAL DETAILS

2.1 Inks and their preparations

Commercially available Prussian blue conductive Carbon ink (C2070424P2, Gwent Group, Pontypool, UK) was used as electrode materials for 3D printing. The ink for the enzyme is prepared through mixing of 6 mL of tetraethoxysilane (TEOS), 1.32 mL of DI water, 1.32 mL of ethanol, and 100 µL of HCl (1.0 M) for 1 h to make a sol-gel (pH 5.0). A 100 µL of the enzyme solution (30 mg of GOx, EC 1.1.3.4, 150 units/mg) was added into 1.0 mL of the sol-gel. Subsequently, this mixture was added to 5 mL of 8% hydroxypropyl cellulose and sonicated for another 10 min. The entire composite was cooled for 6 h prior to printing. Both inks were then transferred to 3 cc syringe barrel as shown in the **Figure S4.**

2.2 Characterization of the ink rheology

The rheological properties of electrochemical electrode and Enzyme inks were characterized using a strain-controlled rheometer (TA instruments, ARES-G2) in the cone and plate configuration (50 mm diameter, 0.0196 rad cone angle). Two different tests were applied to both inks: an amplitude sweep test to characterize plateau elastic (storage) and loss moduli and a frequency sweep test to understand viscoelastic response of the printable inks. The test setup requires loading both inks at a volume of 0.6 ml using a syringe. To avoid the solvent evaporation during testing, a low viscosity mineral oil was applied around the circumference of the plate. The amplitude sweep test was conducted at a constant oscillation frequency of 50 rad/s and an oscillation strain range of 0.0052% to 1000%. The minimum oscillation strains in linear region of amplitude sweep of magnitude 5 % and 0.25% were chosen in frequency sweep test which was applied for Enzyme and Electrode inks, respectively. Here, the angular frequency was increased from 0.01 to 628 rad/s. The cone-plate distance was kept 0.047 mm for all tests and temperature was maintained at room temperature.

2.3 Direct-Ink-Writing

As shown in **Figure 1a**, a custom-built DIW platform was utilized for DIW of the sensors. This platform consists of a three-axis motion system (Aerotech ANT180-ANT130 motion stage) which is capable of positioning the substrate with sub-micron accuracy within a working space of 210 mm x 160 mm x 110 mm. A positive pressure pump (Nscrypt Smart Pump®) is used to dispense the inks. The inks were introduced into a needle valve with a stainless-steel nozzle of 200 µm diameter attached to the pump outlet and their flow were controlled through the pump. A CCD camera attached to the print head was used to monitor the printing process. The inks were printed on a temporary tattoo paper (HPS LLC, Rhome, TX) as a substrate.

Schematic illustration of DIW of electrode and enzyme inks is shown in **Figures 1d-f**. Here, we used a novel approach for printing Enzyme with electrochemical electrodes in a two-step process. Three different sizes were used for electrode printing. Three electrodes with 1 mm (small), 2 mm (medium) and 4 mm (large) diameters and 32 mm long legs were designed in CADFusion (Aerotech Inc) software and the corresponding G-codes were generated. The generated G-code was transferred through a LabVIEW interface to our custom-built DIW system with adjusted air pressure and printing distance to the substrate. **Figure 1b** shows microscopy image of printing of the carbon-mediated ink. The printed electrodes were dried in a vacuum oven at 100 ^{o}C for about 10 minutes prior to enzyme printing. As it has been shown in **Figure 1c**, the enzyme inks were then printed on dried carbon electrode. The **Table S1** in the supporting information summarizes the printing parameters used for this process.

2.4 Screen Printing

To evaluate the effectiveness of the DIW approach in electrode fabrication, we also fabricated the same electrode (i.e. same material and design) using the conventional screen printing approach. The approach used for this purpose is shown in **Figure S5.** The electrode mask was made by laser cutting corresponding designs out of tattoo paper and it was placed on the top of the main papers. Then, screen printed electrodes were fabricated by casting mediated carbon ink over the mask using micrometer adjustable film applicator (EQ-Se-KTQ-100 from MTI Corporation).

2.5 Scanning Electrode Microscopy and Optical Profilometry of 3D printed and screen-printed electrodes

As shown in **Figures 2a-d**, the surface morphology of both 3D printed electrodes and screen-printed ones were characterized through an environmental scanning electron microscopy (FEI Quanta 200F). The interface morphologies between the electrode and enzyme for both 3D printed and screen-printing methods have also been shown. The surface topographies of both electrodes were also characterized using an optical profilometer (Zygo NewView 7300) through white light interferometry. For each electrode, about 2 mm long section was measured to characterize its cross-sectional profile with sub-nm height and sub-micron width resolution. **Figures 2e-f** show surface profiles of screen-printed and 3D printed electrodes, respectively.

2.6 Electrochemical analysis instrumentation

Cyclic voltammetry (CV) and Chronoamperometric (CA) measurements were

performed by using CHI 660E electrochemical workstation (CH Instruments Inc., Austin, TX, USA). A three-electrode cell with a platinum counter electrode and an Ag/AgCl reference electrode was used for electrochemical measurements. All experiments were performed using a 0.1 M phosphate buffer (PBS) (pH 7.4) solution. The operating potential for the 3D printed sensor was selected by using cyclic voltammetry. During the CV measurement, initial potential was 0.0 V, and the initial scan direction was negative. The amperometric detections were recorded after 120 s incubation in the sample solution, using a potential of 0.25 V (vs Ag/ AgCl) for 120 s. The sensor specificity was examined in the presence of common interfering electroactive species: 100 μM ascorbic acid and 100 μM uric acid. All experiments were conducted at room temperature.

3. RESULTS AND DISCUSSION

3.1 Electrode manufacturing

The results of the rheological characterization of mediated carbon and enzyme inks are shown in **Figures 2h-j**. From amplitude sweep test, as shown in **Figure 2h**, the plateau elastic moduli for the carbon and enzyme inks were found to be around 1kPa. Having higher storage modulus compared with loss modulus at low shear rate represents the printability into 3D structures of both electrode and enzyme inks [32]. In other words, both inks have more solid-like behavior compared to viscous liquid-like behavior at such low shear rates which are experienced by inks right after their extrusion. Shear thinning behavior of both viscoelastic inks was captured by frequency sweep test as depicted in **Figure 2i-j**, indicating ideal extrusion characteristics for both inks [33]. As it has been shown in **Figure 2g**, mean height variation through the whole scanning area on screen printed electrode were about twice the corresponding height on DIW electrode. Here, approximately equal projected area for both electrodes were taken as a reference region and the total volume of material for each electrode was calculated. The corresponding results have been shown in **Table 1**. The calculated volumes which represent the amount of material that have been used for each of DIW and screen printing methods. In addition, as shown in **Figures 2a-d**, the Environmental Scanning Electron Microscopy (SEM) measurements have also confirmed the uniformity and homogeneity of printed electrode without enzyme compared with screen-printed ones. The comparison between the surface morphology of 3D printed electrode (**Figure 2a**) and screen printed one (**Figure 2c**) clearly shows a more uniform distribution of active materials across the similar size scale for the 3D-printed electrode. Also, microscopic observation at the interface between electrode and enzyme, demonstrates that 3D printing of the active materials can lead to a uniform and repeatable distribution of the mediator and enzyme in the final multi-material structure as illustrated by **Figure 2b**. This is primarily associated with the high deposition resolution coupled with ink homogeneity in each printed strand and layer.

3.2 Electrochemical behavior of the 3D printed electrode

To investigate the electrochemical performance of 3D printed Prussian blue modified carbon electrode, cyclic voltammetry (CV) was first conducted in PBS. The

effect of different scan rates on the CV's response of the carbon electrode is shown in **Figure 3a**. With the increase of scan rate from 10 mV s^{-1} to 200 mV s^{-1}, the redox peak current increases gradually. **Figure 3b** shows the peak current versus the sweep rate plot was linear (R^2 = 0.99), implying that the kinetic behavior of the electrode is a surface-confined electrode reaction [34].

Figure 3c shows the hydrodynamic voltammograms, the dependence of the response of 3D-printed Prussian blue modified carbon electrode to 50 µM H_2O_2 upon the applied potential. Normally, the high anodic oxidation potential of hydrogen peroxide (>+0.6 V vs. Ag/AgCl) restricts the specificity of amperometric enzymatic biosensors, due to the interference in the potential range [35]. Prussian blue has been widely used to modify electrodes as an efficient catalyst to lower hydrogen peroxide redox potential [36,37]. In this work, the response to H_2O_2 increases steadily to a voltage of 0.3 V and saturated at higher voltages. The results indicate that the Prussian blue has acted as a mediator and the tendency of Prussian blue undergoing redox reaction has helped to increase the electron transfer at electrode. Generally, the low operating potentials greatly minimize interferences from coexisting electroactive species. We choose 0.25 V as an applied potential in most cases. Therefore, the role of Prussian blue is to help detection of hydrogen peroxide oxidation current at lower potential. **Figure 3d** shows CV curves of electrode in PBS and hydrogen peroxide (H_2O_2) solution at 100 mV s^{-1}. In PBS solution (in the absence of H_2O_2), the oxidizing current is as low, as about 13 µA at 0.25 V. With addition of 50 µM H_2O_2, the oxidation current has increased to 25 µA.

The chronoamperometric (CA) curves of the electrode for different concentration of H_2O_2 solutions are shown in **Figure 4a**. With increasing concentration of H_2O_2, the oxidation current increases linearly. The i–c curves of the electrodes are shown in **Figure 4b**. The 3D-printed electrode works linearly in H_2O_2 solution with a concentration range between 0 and 900 µM. The corresponding regression equation of the linear curve in Figure 4b is calculated as: $i = 1.23e^{-8}c - 6.17e^{-8}$, R^2 = 0.997, where c is the concentration of H_2O_2. The sensitivity is estimated to be 12.3 nA μM^{-1}. For screen printed electrode (red curve in Figure 4b), the corresponding regression equation of the linear plot is: $i = 5.05e^{-9}c - 3.19e^{-9}$, R^2 = 0.997. This electrode worked linearly in H_2O_2 solution with a concentration range between 0 and 700 µM. The sensitivity is estimated to be 5.05 nA μM^{-1}. As shown, the 3D-printed electrode has a boarder linear range than screen printed electrode. Furthermore, the sensitivity of 3D-printed electrode towards H_2O_2 is significantly higher than that of screen printed electrode due to the distinct, smooth conductor edges with minimal defects printed by DIW technique and thus resulting in uniform active material distribution and better surface-level electrochemical reaction [38]. In addition, the results shown in **Table 1** and **Figure S5** demonstrates that DIW can significantly reduce the material waste as compared to screen-printing while fabricating the same sized electrodes including comparable amounts of active materials.

3.3 The performance of the 3D co-printed electrode as a glucose biosensor

The chronoamperometric (CA) curves of 3D-printed glucose biosensors (enzyme layer printed on the electrode) for different concentrations of glucose solutions are

shown in **Figure 4c**. With increasing concentration of glucose, the oxidation current increases linearly. In the inset of **Figure 4c**, the electrode works linearly in glucose solution with a concentration range between 100 and 1000 µM. The corresponding regression equation of the linear plot was: $i = 1.64e^{-8}c - 1.134e^{-7}$, R^2 = 0.998, where c is the concentration of glucose in µM. The sensitivity is estimated to be 17.5 nA μM^{-1}. The detection limit is then calculated (S/N=3) to be 6.9 µM. The reproducibility of 3D-printed electrodes is studied by using different electrodes, with detection of 100 µM of glucose (**Figure S2a**). And the repeatability of 3D-printed biosensors is investigated by using the same electrode, with detection of 100 µM of glucose (**Figure S2b**). The results show that the 3D-printed glucose electrode exhibits satisfactory reproducibility (~3% variations) and excellent repeatability. The effect of physiologically relevant concentrations of common coexisting interfering electroactive species on the sensor response is examined. The results, displayed in **Figure 4d**, highlight the high specificity of the sensor toward glucose in the presence of ascorbic acid and uric acid. The response to 100 µM glucose at +0.25 V is suffered from negligible interference by subsequent addition of 100 µM ascorbic acid and 100 µM uric acid as well as some ions (1 µg mL^{-1}). In overall, the high sensitivity and selectivity demonstrated in **Figure 4d** reflect the coupling of the specific biocatalytic reaction with the low-potential amperometric transduction at the 3D-printed biosensor, due to the help of Prussian blue modified carbon electrode. Besides, these 3D-printed biosensors demonstrate remarkably stable responses. These 3D co-printed biosensors are stored at room temperature. The long-term stability is investigated by performing the CA test, using the same strip, with intermittent usage (4h or overnight) and dry storage at room temperature. As shown in **Figure S3**, no apparent change in the response to 100 µM glucose is observed in this period, indicating that the 3D co-printed biosensors have good stability.

It has been shown in the literature that the electrode geometry significantly influence the biosensor response [39]. DIW approach provides the capability of precisely controlling the electrode geometry and thus, the sensor response. To evaluate the effect of electrode diameter on the sensor response, we printed and examined electrodes with three different diameters. As shown in **Figure S1**, the electrode sensitivity increased with decreasing electrode diameter. This result is consistent with the earlier findings in the literature: Electrodes with a higher perimeter-to-surface area ratio (reciprocal of the radius for a circular electrode) have been found to have a lower impedance and higher charge transfer ability due to both reduced ionic resistance of the electrolyte and a higher flux to the electrode during the electrochemical process [40,41].

Finally, to demonstrate flexibility of the 3D-printed glucose biosensors, the mechanical behavior of 3D printed electrode on a tattoo paper is investigated under multiple bending cycles as shown in **Figure S6**. Here, the printed electrode is bent around a cylindrical template of 27 mm diameter multiple times and was examined under a microscope after the deformation cycles. The corresponding results demonstrate that the integrity of the 3D printed electrode is maintained under repeated flexural deformation.

4. CONCLUSION

A novel approach for additive manufacturing flexible glucose biosensors has been demonstrated. Commercial carbon ink modified with Prussian blue as electron transfer mediator, and a custom-made enzyme ink were 3D-printed on a tattoo paper using DIW method. The rheological properties and surface morphology of 3D-printed electrodes were characterized thereafter, and their electrochemical performance was investigated and compared with the conventional screen-printed electrodes having the same geometry and material composition. Results show that 3D-printed electrodes have more uniform and defect free surface which has led them to be more sensitive to electrochemical sensing [42,43]. The *in vitro* characterization of the 3D-printed glucose biosensors revealed their ability to detect micro-molar levels of glucose in the presence of common interfering chemical species. It also shows that using DIW instead of conventional screen printing can save time and material, reducing overall cost. 3D-printed biosensor exhibited better reproducibility, repeatability and long-term stability.

Broader practical utilization of the presented technology will require integration of the printed biosensors with other electronic components for powering the sensor, signal processing and wireless communication on a wearable platform. It should be emphasized that the use of DIW for sensor fabrication also streamlines such an integration task given the recent emergence of printed electronics. Through the DIW approach, the biosensor, associated interconnects, passive electronic components and antennae can be fabricated using a single process which can also be combined with IC integration [44,45], all on a flexible substrate. This critical advance will substantially reduce the cost and increase the sophistication of biosensors for personal health monitoring. Our future efforts will be aimed at realizing such a complete integration and using the packaged system in long term, *in vivo* glucose monitoring.

AUTHOR INFORMATION

Corresponding Authors

* E-mail: arda.gozen@wsu.edu; Yuehe.lin@wsu.edu

1 These authors contributed equally to this work.

Notes

The authors declare no competing financial interest.

ACKNOWLEDGMENT

This work was supported by start-up fund of Washington State University.

Reference

[1] J. Wang, Electrochemical Glucose Biosensors Electrochemical Glucose Biosensors, 108 (2008) 814–825. doi:10.1021/cr068123a.

[2] A.-L. Hu, Y.-H. Liu, H.-H. Deng, G.-L. Hong, A.-L. Liu, X.-H. Lin, X.-H. Xia, W. Chen, Fluorescent hydrogen peroxide sensor based on cupric oxide nanoparticles and its application for glucose and l-lactate detection, Biosens. Bioelectron. 61 (2014) 374–378. https://www.sciencedirect.com/science/article/pii/S0956566314003893?via%3Dihub (accessed May 8, 2018).

[3] L. Lin, X. Song, Y. Chen, M. Rong, T. Zhao, Y. Wang, Y. Jiang, X. Chen, Intrinsic peroxidase-like catalytic activity of nitrogen-doped graphene quantum dots and their application in the colorimetric detection of H2O2 and glucose, Anal. Chim. Acta. 869 (2015) 89–95. https://www.sciencedirect.com/science/article/pii/S0003267015002020?via%3Dihub (accessed May 8, 2018).

[4] J. Yuan, Y. Cen, X.-J. Kong, S. Wu, C.-L. Liu, R.-Q. Yu, X. Chu, MnO 2 -Nanosheet-Modified Upconversion Nanosystem for Sensitive Turn-On Fluorescence Detection of H 2 O 2 and Glucose in Blood, ACS Appl. Mater. Interfaces. 7 (2015) 10548–10555. http://pubs.acs.org/doi/10.1021/acsami.5b02188 (accessed May 8, 2018).

[5] T.J.D.R.F.C.G.M.S. Group, Continuous Glucose Monitoring and Intensive Treatment of Type 1 Diabetes, N. Engl. J. Med. 359 (2008) 1464–1476. http://www.nejm.org/doi/abs/10.1056/NEJMoa0805017 (accessed November 16, 2017).

[6] D.-H. Kim, R. Ghaffari, N. Lu, J.A. Rogers, Flexible and Stretchable Electronics for Biointegrated Devices, Annu. Rev. Biomed. Eng. 14 (2012) 113–128. http://www.ncbi.nlm.nih.gov/pubmed/22524391 (accessed November 16, 2017).

[7] A.J. Bandodkar, J. Wang, Non-invasive wearable electrochemical sensors: a review, Trends Biotechnol. 32 (2014) 363–371. http://www.ncbi.nlm.nih.gov/pubmed/24853270 (accessed November 16, 2017).

[8] H. Wang, L. Zhang, Y. Jiang, L. Chen, Z. Duan, X. Lv, S. Zhu, A sandwiched electroanalysis method for probing Anthrax DNAs based on glucose-induced gold growth and catalytic coupling of tyramine using gold-mineralized glucose oxidase, Sensors Actuators, B Chem. 261 (2018) 441–450. doi:10.1016/j.snb.2018.01.171.

[9] S. Zhu, X.E. Zhao, J. You, G. Xu, H. Wang, Carboxylic-group-functionalized single-walled carbon nanohorns as peroxidase mimetics and their application to glucose detection, Analyst. 140 (2015) 6398–6403. doi:10.1039/c5an01104c.

[10] S. Imani, A.J. Bandodkar, A.M.V. Mohan, R. Kumar, S. Yu, J. Wang, P.P. Mercier, A wearable chemical–electrophysiological hybrid biosensing system for real-time health and fitness monitoring, Nat. Commun. 7 (2016) 11650.

http://www.ncbi.nlm.nih.gov/pubmed/27212140 (accessed November 16, 2017).

[11] S. Gong, W. Schwalb, Y. Wang, Y. Chen, Y. Tang, J. Si, B. Shirinzadeh, W. Cheng, A wearable and highly sensitive pressure sensor with ultrathin gold nanowires, Nat. Commun. 5 (2014) 3132. http://www.ncbi.nlm.nih.gov/pubmed/24495897 (accessed November 16, 2017).

[12] T.Q. Trung, N.-E. Lee, Flexible and Stretchable Physical Sensor Integrated Platforms for Wearable Human-Activity Monitoringand Personal Healthcare, Adv. Mater. 28 (2016) 4338–4372. http://doi.wiley.com/10.1002/adma.201504244 (accessed November 16, 2017).

[13] W. Gao, S. Emaminejad, H.Y.Y. Nyein, S. Challa, K. Chen, A. Peck, H.M. Fahad, H. Ota, H. Shiraki, D. Kiriya, D.-H. Lien, G.A. Brooks, R.W. Davis, A. Javey, Fully integrated wearable sensor arrays for multiplexed in situ perspiration analysis, Nature. 529 (2016) 509–514. http://www.ncbi.nlm.nih.gov/pubmed/26819044 (accessed November 16, 2017).

[14] S. Savagatrup, E. Chan, S.M. Renteria-Garcia, A.D. Printz, A. V. Zaretski, T.F. O'Connor, D. Rodriquez, E. Valle, D.J. Lipomi, Plasticization of PEDOT:PSS by Common Additives for Mechanically Robust Organic Solar Cells and Wearable Sensors, Adv. Funct. Mater. 25 (2015) 427–436. http://doi.wiley.com/10.1002/adfm.201401758 (accessed November 16, 2017).

[15] S. Imani, A.J. Bandodkar, A.M.V. Mohan, R. Kumar, S. Yu, J. Wang, P.P. Mercier, A wearable chemical–electrophysiological hybrid biosensing system for real-time health and fitness monitoring, Nat. Commun. 7 (2016) 11650. http://www.nature.com/doifinder/10.1038/ncomms11650 (accessed May 7, 2018).

[16] A. Abellán-Llobregat, I. Jeerapan, A. Bandodkar, L. Vidal, A. Canals, J. Wang, E. Morallón, A stretchable and screen-printed electrochemical sensor for glucose determination in human perspiration, Biosens. Bioelectron. 91 (2017) 885–891. https://www.sciencedirect.com/science/article/pii/S0956566317300581 (accessed May 7, 2018).

[17] A.J. Bandodkar, W. Jia, C. Yardımcı, X. Wang, J. Ramirez, J. Wang, Tattoo-Based Noninvasive Glucose Monitoring: A Proof-of-Concept Study, Anal. Chem. 87 (2015) 394–398. doi:10.1021/ac504300n.

[18] J.T. Muth, D.M. Vogt, R.L. Truby, Y. Mengüç, D.B. Kolesky, R.J. Wood, J. a. Lewis, Embedded 3D printing of strain sensors within highly stretchable elastomers, Adv. Mater. (2014) 6307–6312.

[19] M. Wei, F. Zhang, W. Wang, P. Alexandridis, C. Zhou, G. Wu, 3D direct writing fabrication of electrodes for electrochemical storage devices, J. Power Sources. 354 (2017) 134–147. http://dx.doi.org/10.1016/j.jpowsour.2017.04.042.

[20] A.B. Dababneh, I.T. Ozbolat, Bioprinting Technology: A Current State-of-the-Art Review, J. Manuf. Sci. Eng. 136 (2014) 061016.

http://manufacturingscience.asmedigitalcollection.asme.org/article.aspx?doi=10.1115/1.4028512.

[21] J. Sun, W. Zhou, D. Huang, J.Y.H. Fuh, G.S. Hong, An Overview of 3D Printing Technologies for Food Fabrication, Food Bioprocess Technol. 8 (2015) 1605–1615.

[22] S. Nesaei, M. Rock, Y. Wang, Additive Manufacturing with Conductive , Viscoelastic Polymer Composites : Direct- Ink-Writing of Electrolytic and Anodic Poly (ethylene oxide) Composites, J. Manuf. Sci. Eng. Addit. (2017) 1–52.

[23] J.E. Smay, J. Cesarano, J.A. Lewis, Colloidal inks for directed assembly of 3-D periodic structures, Langmuir. 18 (2002) 5429–5437.

[24] R. Cornock, S. Beirne, G.G. Wallace, Development of a Coaxial Melt Extrusion Printing process for specialised composite bioscaffold fabrication, 2013 IEEE/ASME Int. Conf. Adv. Intell. Mechatronics Mechatronics Hum. Wellbeing, AIM 2013. (2013) 973–978. doi:10.1109/AIM.2013.6584220.

[25] J.O. Hardin, T.J. Ober, A.D. Valentine, J.A. Lewis, Microfluidic Printheads for Multimaterial 3D Printing of Viscoelastic Inks, Adv. Mater. (2015) 3279–3284.

[26] M.A. Skylar-Scott, S. Gunasekaran, J.A. Lewis, Laser-assisted direct ink writing of planar and 3D metal architectures, Proc. Natl. Acad. Sci. 113 (2016) 6137–6142. http://www.pnas.org/lookup/doi/10.1073/pnas.1525131113.

[27] M.K. Hausmann, P.A. Rühs, G. Siqueira, R. Libanori, T. Zimmermann, A.R. Studart, Dynamics of Cellulose Nanocrystal Alignment during 3D Printing, ACS Nano. (2018).

[28] J.P. Lewicki, J.N. Rodriguez, C. Zhu, M.A. Worsley, A.S. Wu, Y. Kanarska, J.D. Horn, E.B. Duoss, J.M. Ortega, W. Elmer, R. Hensleigh, R.A. Fellini, M.J. King, 3D-Printing of Meso-structurally Ordered Carbon Fiber/Polymer Composites with Unprecedented Orthotropic Physical Properties, Sci. Rep. 7 (2017) 43401. http://www.nature.com/articles/srep43401.

[29] B.Y. Ahn, E.B. Duoss, M.J. Motala, X. Guo, S.-I. Park, Y. Xiong, J. Yoon, R.G. Nuzzo, J. a Rogers, J. a Lewis, Omnidirectional printing of flexible, stretchable, and spanning silver microelectrodes., Science. 323 (2009) 1590–3. doi:10.1126/science.1168375.

[30] R.D. Farahani, M. Dubé, D. Therriault, Three-Dimensional Printing of Multifunctional Nanocomposites: Manufacturing Techniques and Applications, Adv. Mater. (2016) 5794–5821. doi:10.1002/adma.201506215.

[31] K. Tian, J. Bae, S.E. Bakarich, C. Yang, R.D. Gately, G.M. Spinks, M. in het Panhuis, Z. Suo, J.J. Vlassak, 3D Printing of Transparent and Conductive Heterogeneous Hydrogel-Elastomer Systems, Adv. Mater. (2017) 1604827. doi:10.1002/adma.201604827.

[32] R.L. Truby, J.A. Lewis, Printing soft matter in three dimensions, Nature. 540 (2016) 371–378. doi:10.1038/nature21003.

[33] J. a. Lewis, Direct Ink Writing of 3D Functional Materials, Adv. Funct. Mater. 16 (2006) 2193–2204. doi:10.1002/adfm.200600434.

[34] H. Yang, M.T. Rahman, D. Du, R. Panat, Y. Lin, 3-D printed adjustable

microelectrode arrays for electrochemical sensing and biosensing, Sensors Actuators, B Chem. 230 (2016) 600–606. http://dx.doi.org/10.1016/j.snb.2016.02.113.

[35] V. Laurinavicius, B. Kurtinaitiene, R. Stankeviciute, Behavior of PQQ Glucose Dehydrogenase on Prussian Blue□Modified Carbon Electrode, Electroanalysis. 20 (2008) 1391–1395. http://doi.wiley.com/10.1002/elan.200804216 (accessed January 17, 2018).

[36] S. Banerjee, P. Sarkar, A.P.F. Turner, Amperometric biosensor based on Prussian Blue nanoparticle-modified screen-printed electrode for estimation of glucose-6-phosphate, Anal. Biochem. 439 (2013) 194–200. doi:10.1016/J.AB.2013.04.025.

[37] Y. Liu, Z. Chu, Y. Zhang, W. Jin, Amperometric glucose biosensor with high sensitivity based on self-assembled Prussian Blue modified electrode, Electrochim. Acta. 54 (2009) 7490–7494. https://www.sciencedirect.com/science/article/pii/S0013468609010391 (accessed January 17, 2018).

[38] G. Li, P. Miao, Theoretical Background of Electrochemical Analysis, in: 2013: pp. 5–18. http://link.springer.com/10.1007/978-3-642-34252-3_2 (accessed January 1, 2018).

[39] Y. Lin, F. Lu, Y. Tu, Z. Ren, Glucose Biosensors Based on Carbon Nanotube Nanoelectrode Ensembles, Nano Lett. 4 (2004) 191–195. http://pubs.acs.org/doi/abs/10.1021/nl0347233 (accessed December 31, 2017).

[40] S.F. Cogan, J. Ehrlich, T.D. Plante, The effect of electrode geometry on electrochemical properties measured in saline, 2014 36th Annu. Int. Conf. IEEE Eng. Med. Biol. Soc. EMBC 2014. (2014) 6850–6853.

[41] Z.C. Kennedy, J. Christ, K. Evans, B. Arey, L. Sweet, M.G. Warner, R. Erikson, C.A. Barrett, 3D-Printed Poly(vinylidene fluoride)/Carbon Nanotube Composites as a Tuneable, Low-Cost Chemical Vapour Sensing Platform, Nanoscale. (2017). http://pubs.rsc.org/en/Content/ArticleLanding/2017/NR/C7NR00617A.

[42] G. Schneider, New generation of graphene biosensors based on smooth surfaces and sharp edges, (n.d.). https://www.universiteitleiden.nl/en/research/research-projects/science/new-generation-of-graphene-biosensors-based-on-smooth-surfaces-and-sharp-edges.

[43] V. Vamvakaki, N.A. Chaniotakis, Immobilization of enzymes into nanocavities for the improvement of biosensor stability, Biosens. Bioelectron. 22 (2007) 2650–2655. https://www.sciencedirect.com/science/article/pii/S0956566306005331 (accessed December 6, 2017).

[44] B. Li, P. a Clark, K.H. Church, Robust Direct-Write Dispensing Tool and Solutions for Micro/Meso-Scale Manufacturing and Packaging, ASME_IEEE Int. Manuf. Sci. Eng. Conf. (2007) 1–7. doi:10.1115/MSEC2007-31037.

[45] P. Deffenbaugh, K. Church, E. Paso, J. Goldfarb, X. Chen, A. Manufacturing, D. Printing, Fully 3D Printed 2 . 4 GHz Bluetooth / Wi-Fi Antenna Key words

III . Printed RF Antenna on Liquid Crystal, (n.d.) 1–7.

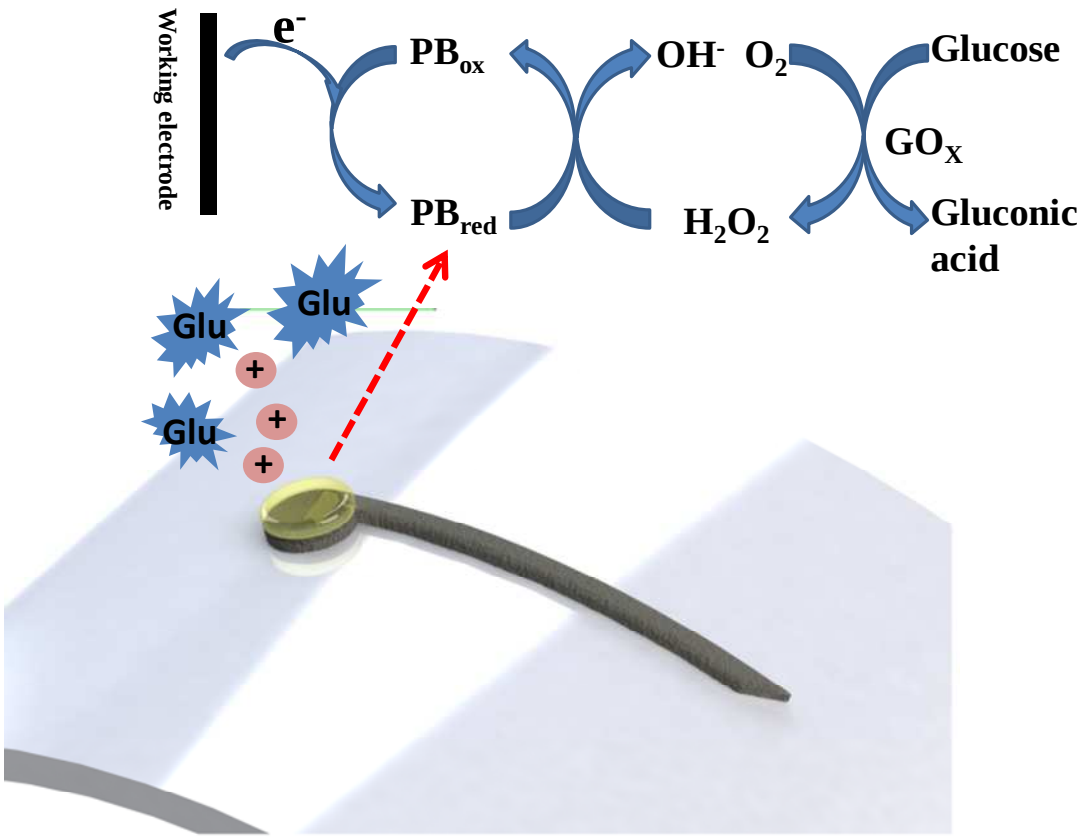

Scheme 1. 3D printed biosensor for glucose sensing.

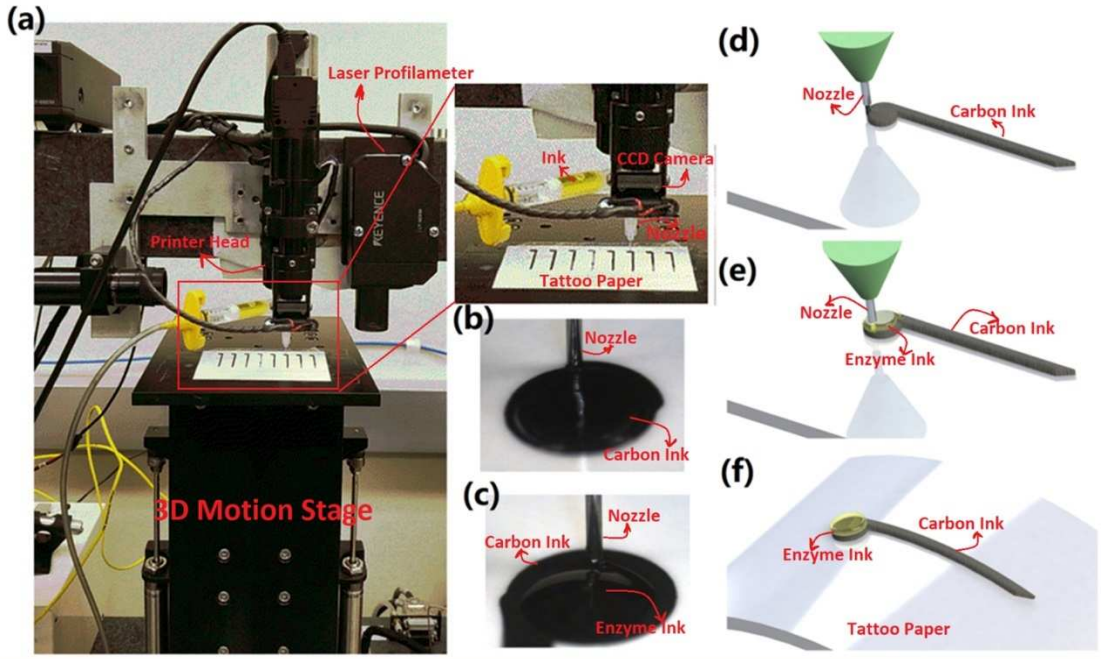

Figure 1. Schematic illustration of Direct-Ink-Writing of Electrode and Enzyme Ink: (a) Custom-made Direct-Ink-Write system. (b) DIW of carbon-mediated ink (c) DIW of enzyme ink. (d) Electrode printing. (e) Enzyme printing. (f) 3D printed glucose biosensor on flexible substrate.

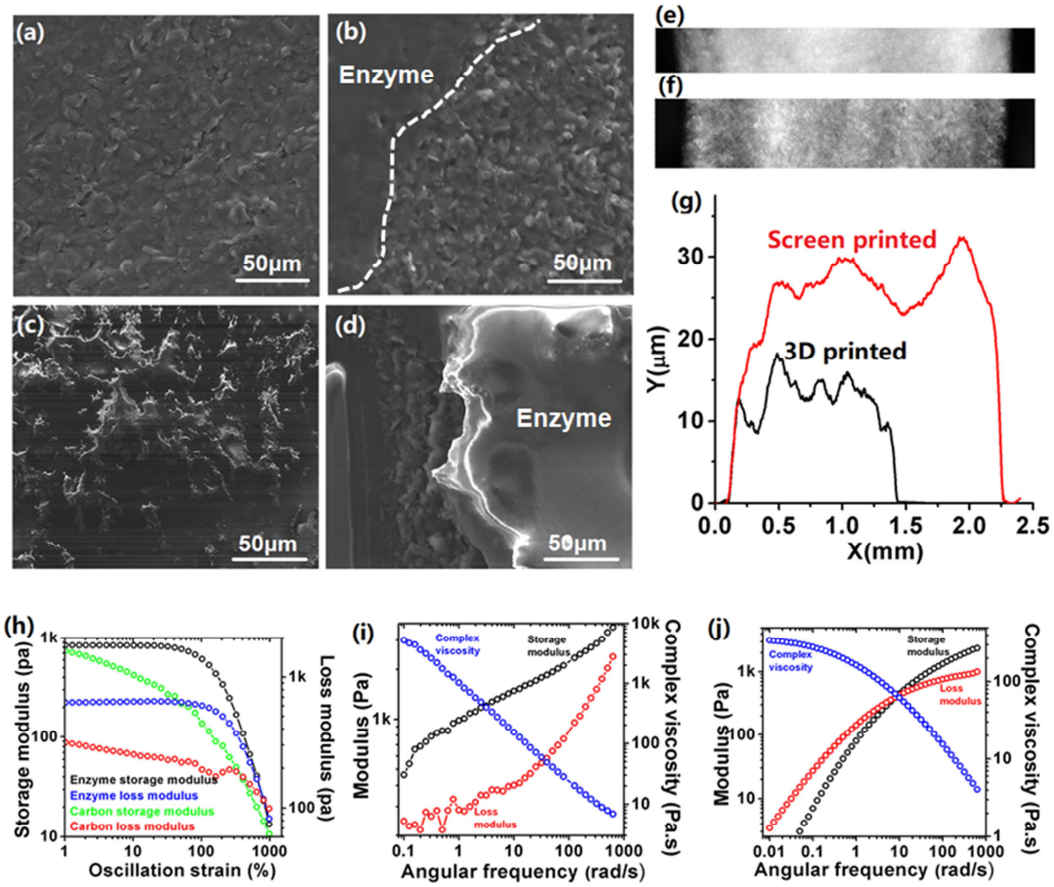

Figure 2. Scanning Electron Microscopy (SEM) images of 3D printed and screen-printed Electrodes and Enzyme layers: (a) 3D Printed electrode; (b) 3D Printed electrode with enzyme layer; (c) screen-printed electrode; (d) screen printed electrode with enzyme layer; Optical profilometry (Zygo) of screen-printed and 3D printed electrodes: (e) image of screen printed electrode; (f) image of 3D printed electrode; (g) Mean cross-sectional profile of screen printed electrode (red) and 3D printed electrode (black); (h) Modulus versus strain oscillation from Amplitude sweep test for both electrode and enzyme inks; (i) Modulus and Complex Viscosity versus angular frequency from frequency sweep test for electrode ink; (j) Modulus and Complex viscosity versus angular frequency from frequency sweep test for enzyme ink;

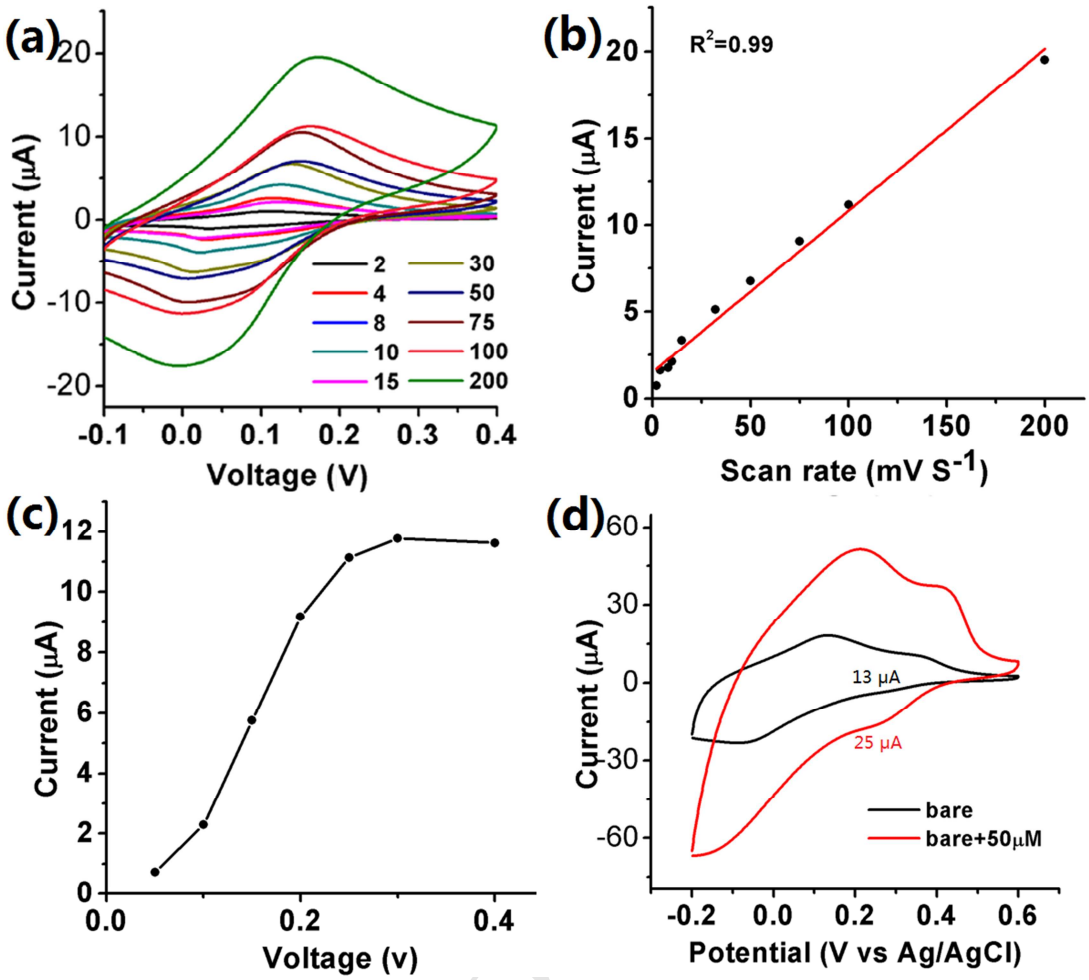

Figure 3. (a) Cyclic voltammograms of 3D printed electrode in PBS solution with variation of scan rates. (b) The fitting curves of peak current vs. scan rate in Figure 3(a). (c) Hydrodynamic voltammograms for 50 μM of H_2O_2 at 3D printed electrode. Voltammograms were recorded by applying the appropriate potential and allowing the transient current to decay prior to the H_2O_2 addition. (d) 3D printed electrode response to 50 μM of H_2O_2. The scan rate is 100 mV $s^{-1}$and the reference electrode is Ag/AgCl.

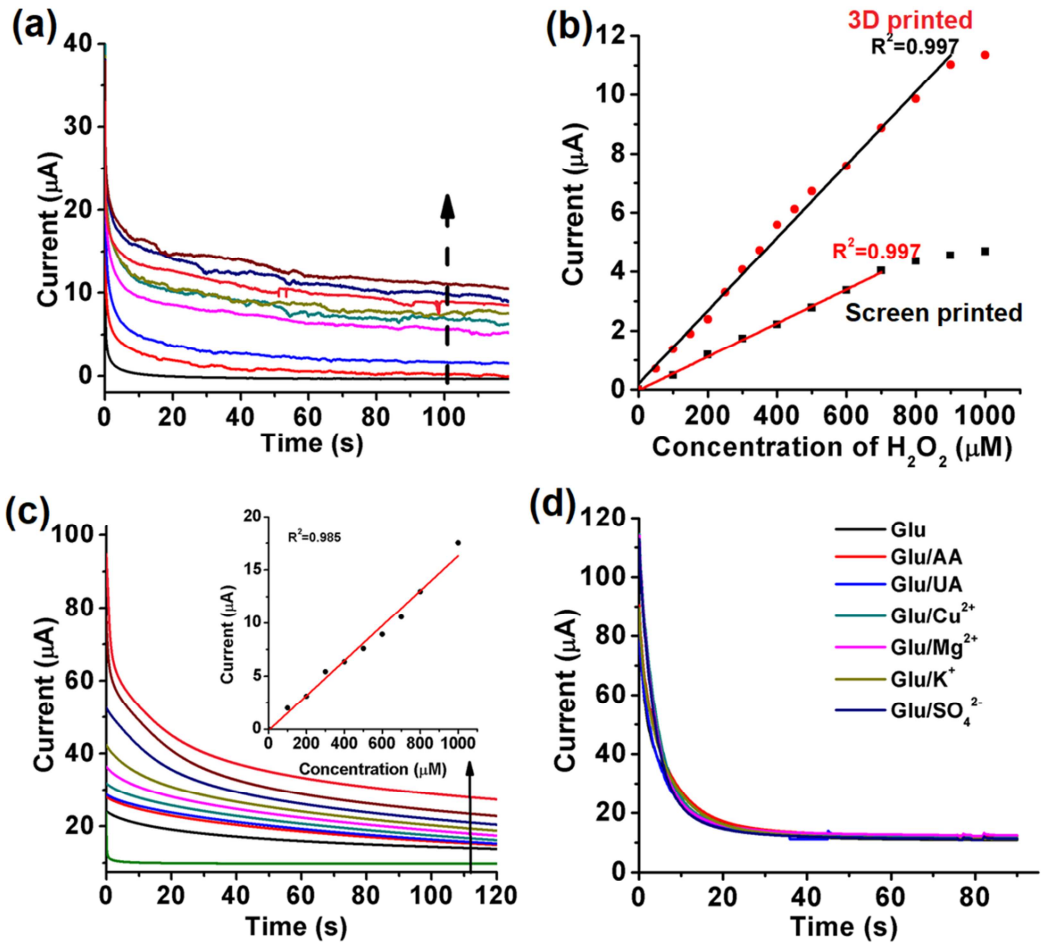

Figure 4. (a) The chronoamperometric (CA) curves (measured with high potential 0.25 V vs. Ag/AgCl) of 3D printed electrode with different concentration of H_2O_2. (b) The i–c curves of the 3D printed electrode (black) and screen-printed electrode (red) derived from CA measurements of H_2O_2. (c) Chronoamperometric response of the 3D printed glucose sensor to increasing glucose concentrations from 0 μM to 1000 μM in PBS solution with 100 μM increments. (d) Interference study in the presence of 100 μM glucose, followed by subsequent additions of 100 μM ascorbic acid, 100 μM uric acid and other interfering substances (1 μg mL^{-1}). Potential step 0 to +0.25 V vs Ag/AgCl.

Table 1. Results of the interferometric measurements regarding the electrode geometries

Statistical Calculations	**DIW Electrode**	**Screen Printed Electrode**
Total projected area (μm^2)	345800	345100
Total material volume (μm^3)	**5263000**	**9253000**
Total projected boundary length (μm)	3053	3017

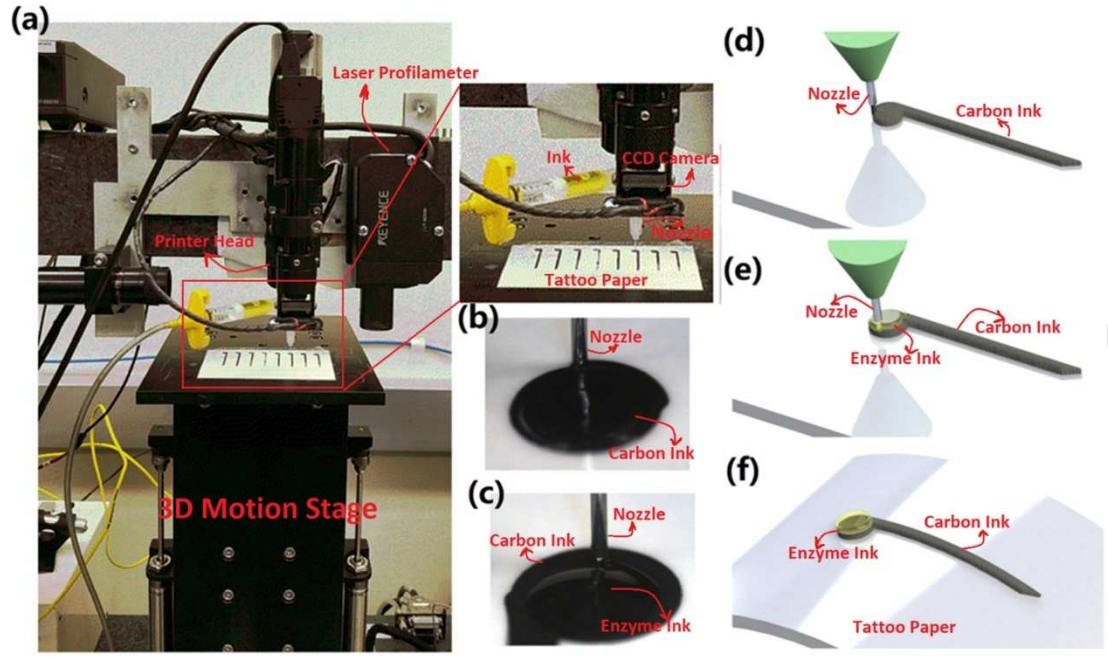

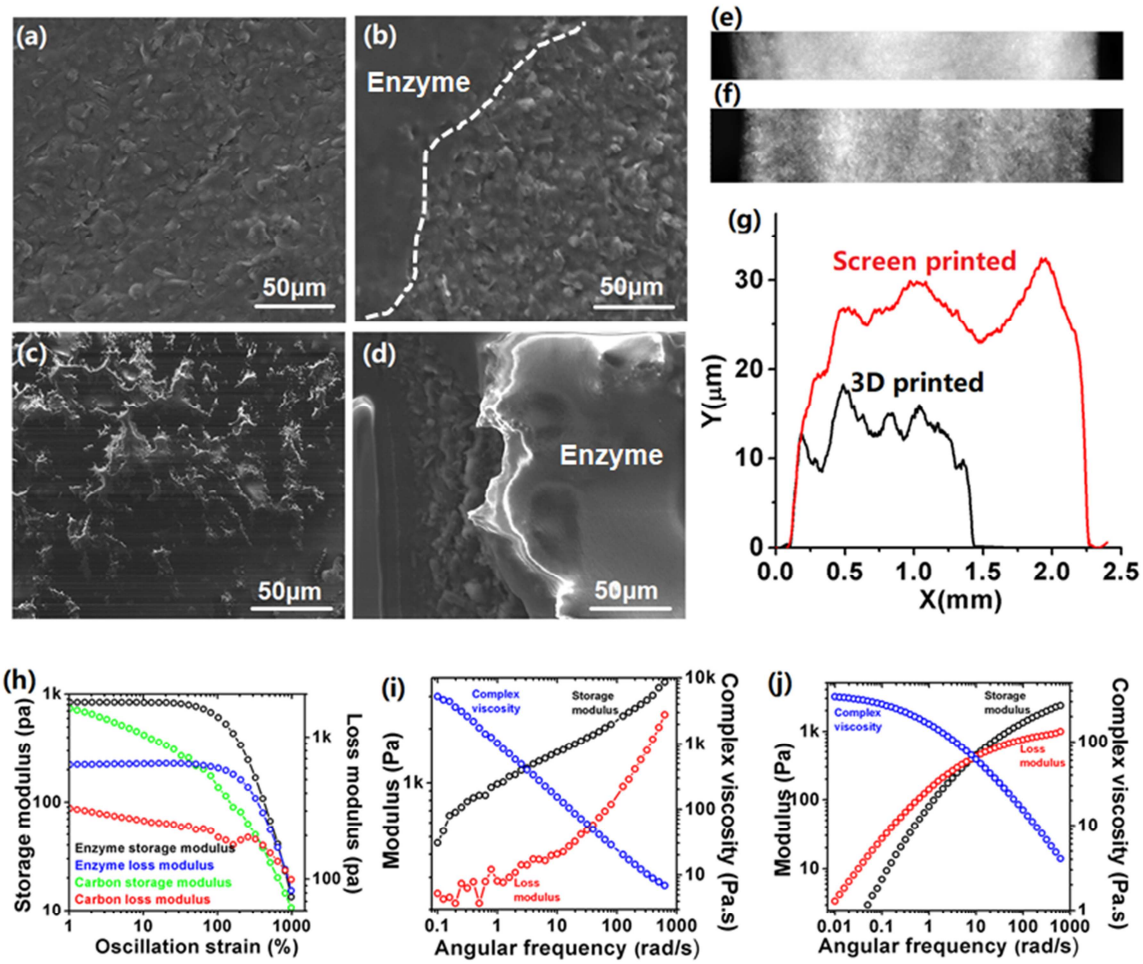
(a)
50μm
(b)
Enzyme
50μm
(c)
50μm
(d)
Enzyme
50μm
(e)
(f)
(g)
Screen printed
3D printed
Y(μm)
X(mm)
(h)
Storage modulus (pa)
Loss modulus (pa)
Enzyme storage modulus
Enzyme loss modulus
Carbon storage modulus
Carbon loss modulus
Oscillation strain (%)
(i)
Complex viscosity
Storage modulus
Loss modulus
Modulus (Pa)
Complex viscosity (Pa.s)
Angular frequency (rad/s)
(j)
Complex viscosity
Storage modulus
Loss modulus
Modulus (Pa)
Complex viscosity (Pa.s)
Angular frequency (rad/s)

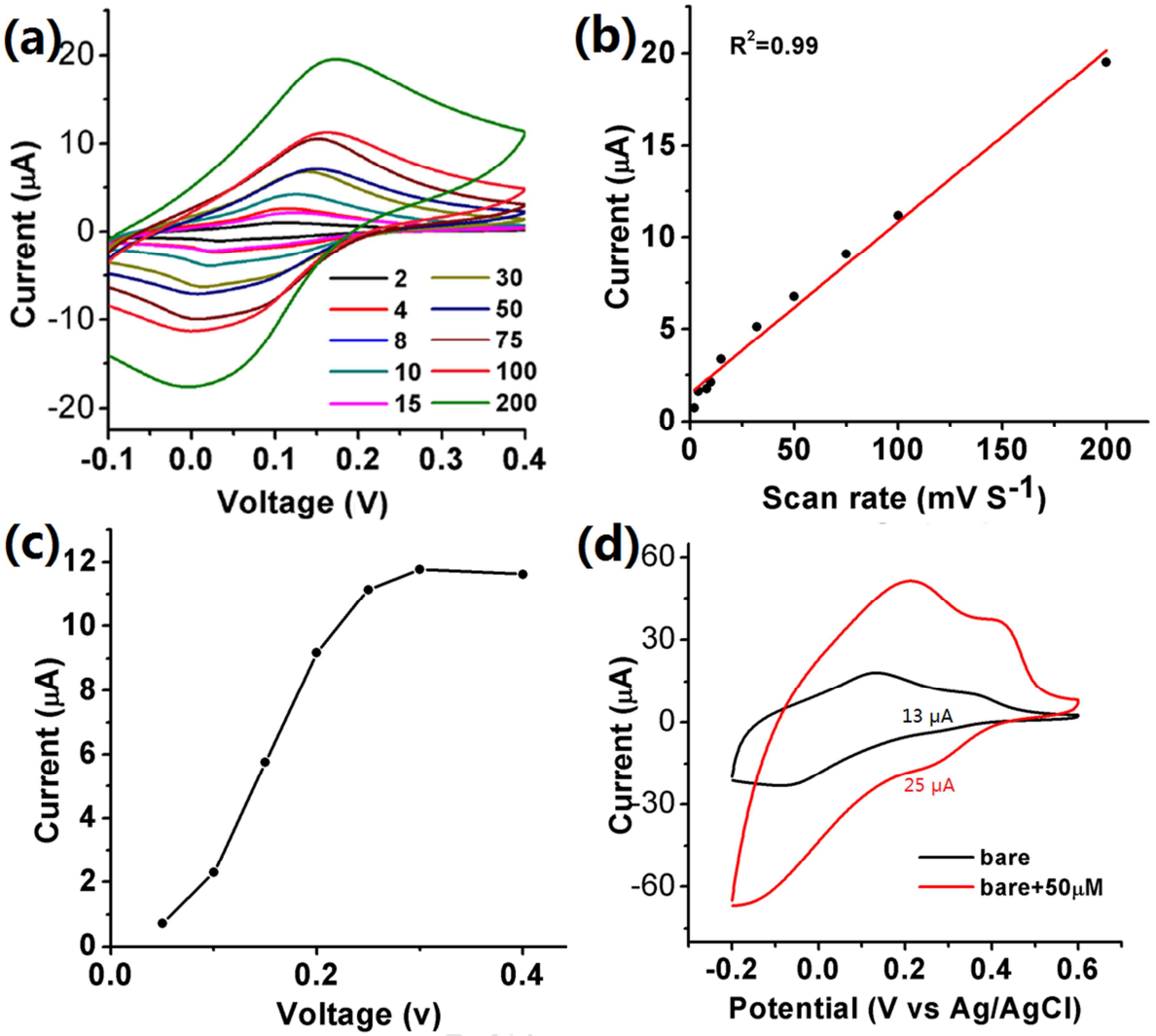
(a)
Current (μA)
Voltage (V)
2
4
8
10
15
30
50
75
100
200
(b)
R²=0.99
Current (μA)
Scan rate (mV S⁻¹)
(c)
Current (μA)
Voltage (v)
(d)
Current (μA)
13 μA
25 μA
bare
bare+50μM
Potential (V vs Ag/AgCl)

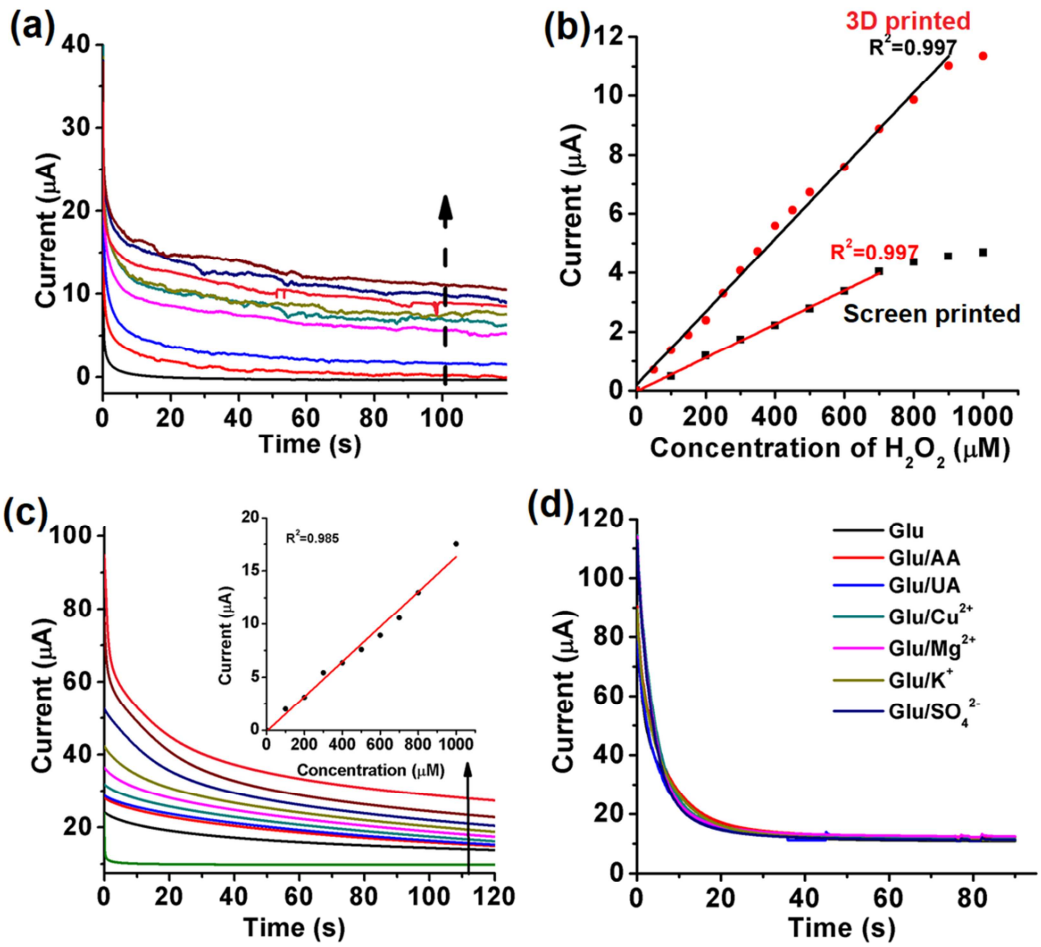
(a)
Current (μA)
Time (s)
(b)
3D printed
R²=0.997
R²=0.997
Screen printed
Current (μA)
Concentration of H2O2 (μM)
(c)
R²=0.985
Current (μA)
Concentration (μM)
Current (μA)
Time (s)
(d)
Glu
Glu/AA
Glu/UA
Glu/Cu2+
Glu/Mg2+
Glu/K+
Glu/SO4 2-
Current (μA)
Time (s)

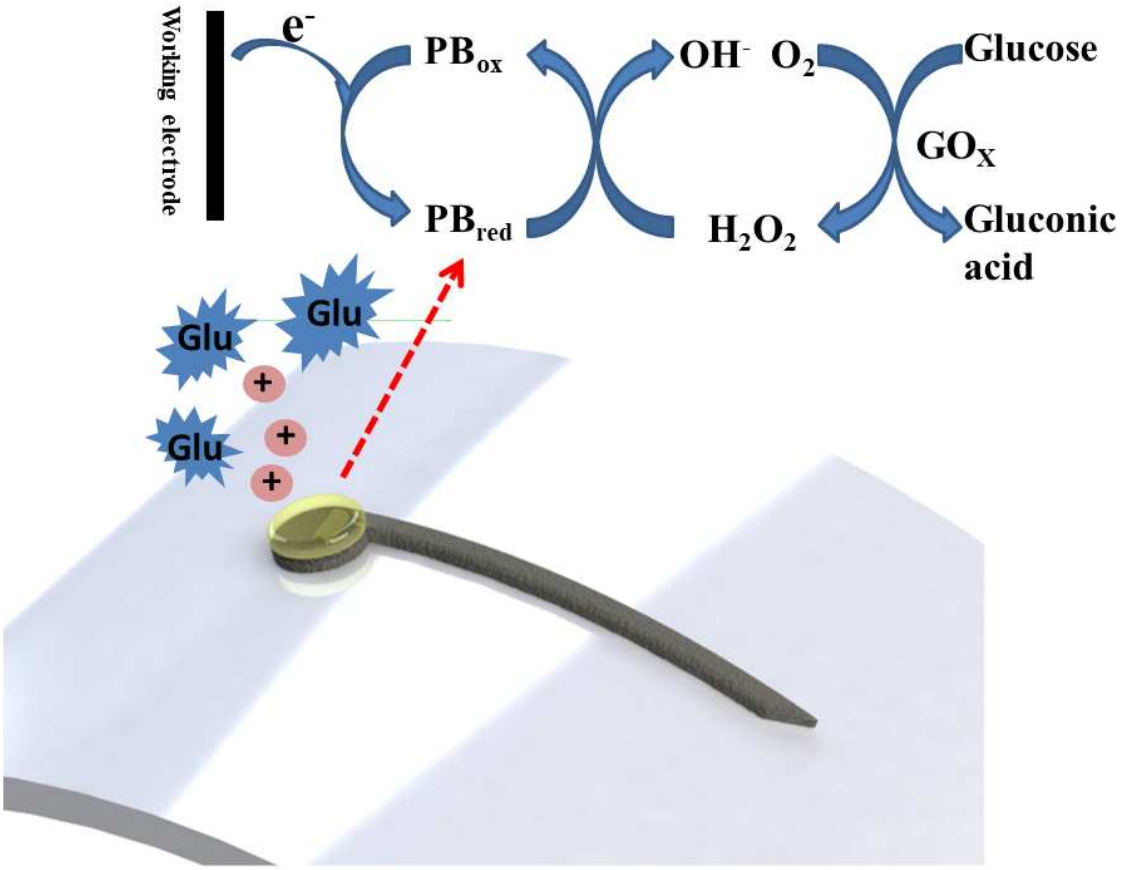

Highlights:

- The first 3D printed flexible electrochemical biosensor for glucose detection.
- 17.5 nA μM^{-1} sensitivity, 6.9 μM detection range (S/N= 3), 100-1000 μM linear range achieved with the printed sensor.
- Improved surface morphology, electrochemical performance and material economy compared to screen printing.

Supporting Information

Micro Additive Manufacturing of Glucose Biosensors: A feasibility study

Sepehr Nesaei [a1], Yang Song [a1], Yijia Wang[a], Xiaofan Ruan[a], Arda Gozen[a] and Yuehe Lin[a]

[a] *School of Mechanical and Materials Engineering, Washington State University, Pullman, WA 99164*
[1] *The authors have equal contributions*

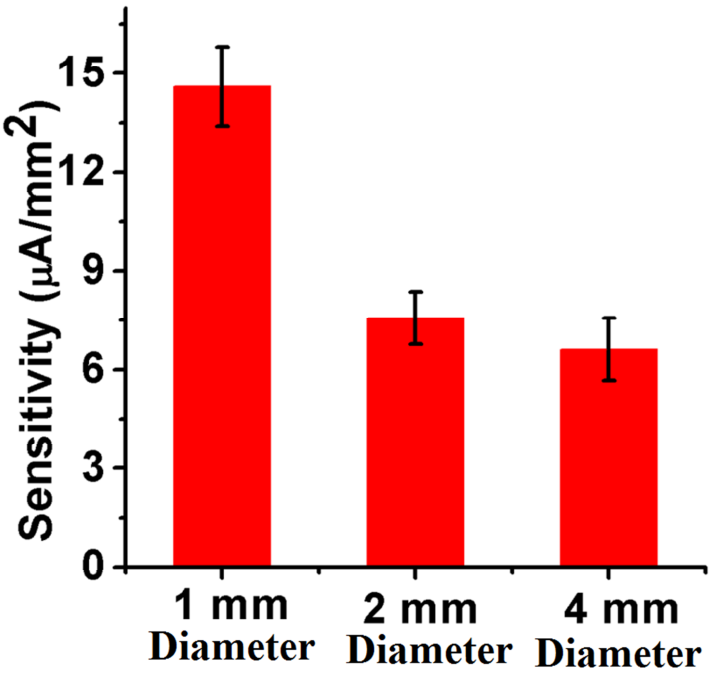

Figure S1. Effect of electrode surface area on the amperometric response of 80 µM H_2O_2 at 3D printed mediated carbon electrodes. Diameter: 1 mm; 2 mm; 4 mm.

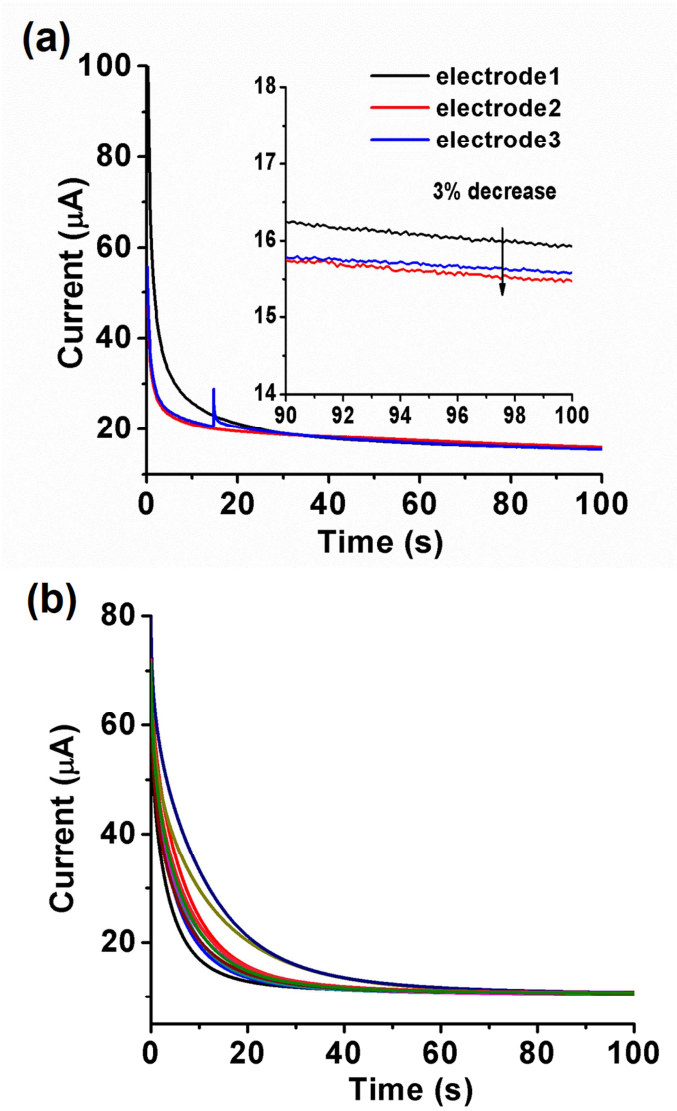

Figure S2. (a) 3D printed electrode reproducibility study in the presence of 100 μM glucose, followed by measuring of different 3D co-printed glucose electrodes. Potential step to +0.25 V vs Ag/AgCl. (b) The repeatability of 3D printed biosensors study in the presence of 100 μM glucose, followed by measuring of one 3D co-printed glucose electrode. Potential step to +0.25 V vs Ag/AgCl.

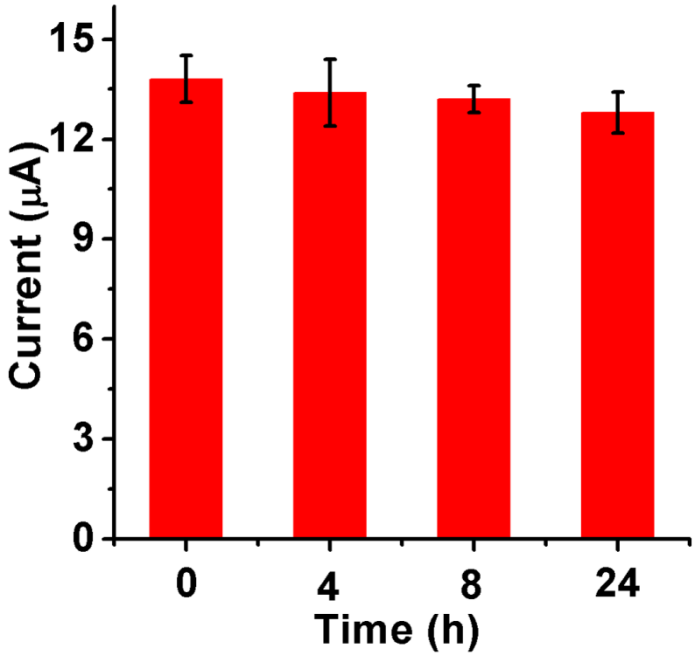

Figure S3. Long-term stability study in the presence of 100 μM glucose recorded on the 3D co-printed glucose electrode with increasing time (0, 4, 8, 12 h).

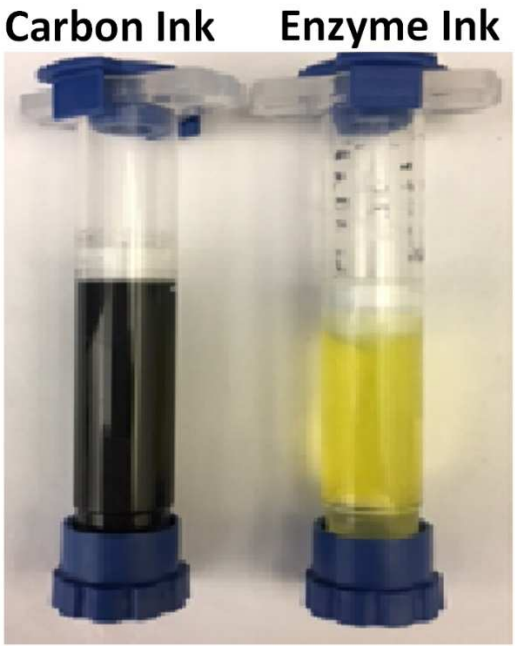

Figure S4. Mediated Carbon Ink and Enzyme Ink in 3mm syringe barrel

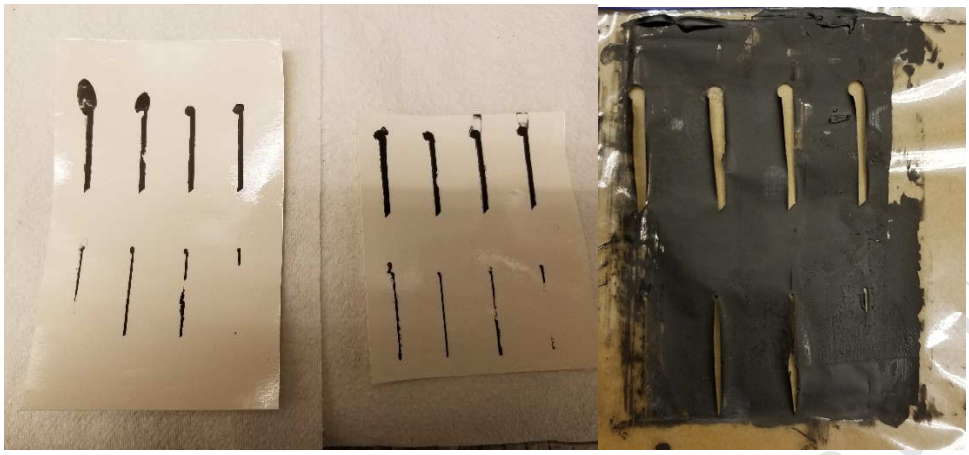

Figure S5. Screen-printed electrodes with their printing mask

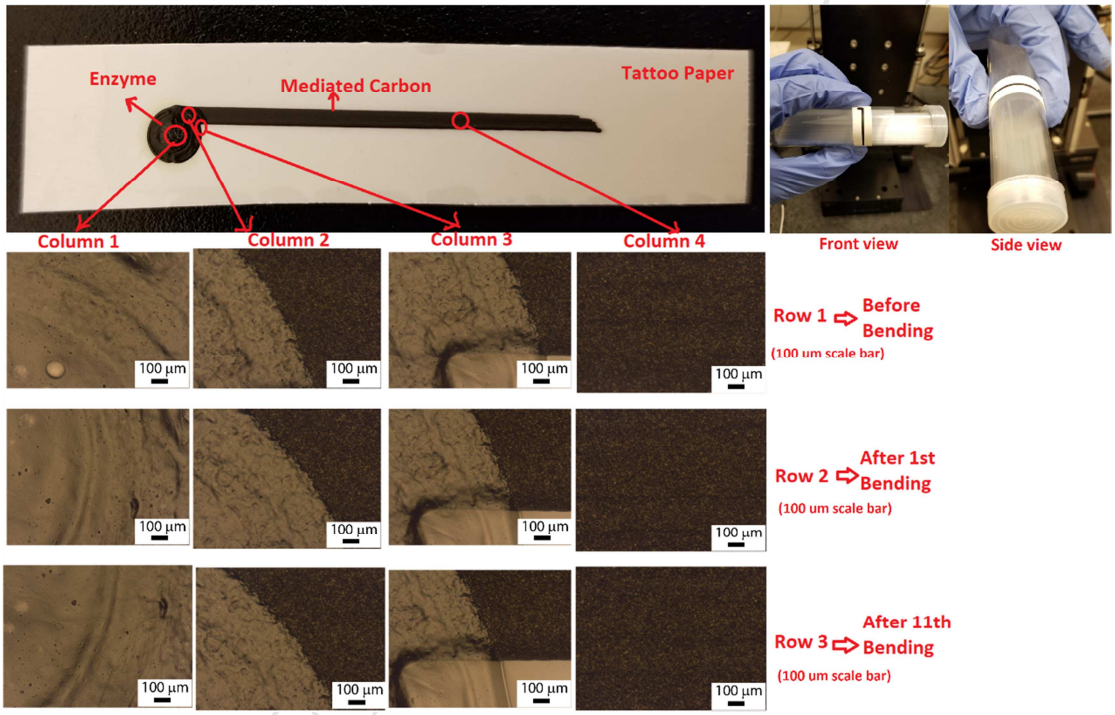

Figure S6. Mechanical Bending of 3D printed glucose biosensor: each column represents one area on 3D co-printed electrode as shown in red circle, each row represents highlighted red areas before, after 1 cycle and after 11 cycles of bending, respectively.

Table S1. Direct-Ink-Writing printing parameters

Type of Printable Ink	Printing Speed (mm/s)	Transition Speed (mm/s)	Applied Pressure (Psi)	Printing Distance to Substrate (µm)	Valve Displacement (mm)	Nozzle Diameter (µm)
Electrode ink	2.5	20	20	100	0.9	200
Enzyme ink	2.5	-	5	100	0.9	200